American Journal of Neural Networks and Applications
2026, Vol. 12, No. 2, pp. 99–109
https://doi.org/10.11648/j.ajnna.20261202.15

Research Article

Joint Compressive Sensing, LDPC Coding, and Neural Network-Based Predistortion for 6G Networks OTFS Transmission System Optimization

Hariniony Bienvenu Rakotonirina[1, *], Randriana Heritiana Nambinina Erica[2], Marie Emile Randrianandrasana[1], Ando Nirina Andriamanalina[2]

[1]Department of Telecommunication, High School Polytechnic of Antsirabe, Antsirabe, Madagascar

[2]Telecommunications, Doctoral School of Engineering Sciences and Innovation, Antananarivo, Madagascar

Abstract

Orthogonal Time Frequency Space (OTFS) modulation has recently emerged as a promising waveform for next-generation wireless communications, particularly in high-mobility environments characterized by doubly selective channels. However, the practical deployment of OTFS systems faces three major challenges: the high Peak-to-Average Power Ratio (PAPR) of multicarrier signals, which induces severe nonlinear distortions in the High-Power Amplifier (HPA); the growing demand for high-data-rate transmission requiring efficient data compression; and the inherently noisy transmission channel that degrades signal integrity. This paper proposes a comprehensive optimization of the OTFS transmission system by synergistically combining three complementary techniques. First, a neural network-based predistortion model is employed to linearize the HPA, enabling high-efficiency operation without signal degradation. Second, Compressive Sensing based on the Lifting Wavelet Transform (LWT) and the ALISTA algorithm is integrated to drastically reduce the volume of transmitted data, down to 10%–30% of the original signal, while ensuring fast and accurate reconstruction. Third, Low-Density Parity-Check (LDPC) coding is incorporated to enhance robustness against channel noise. Simulation results demonstrate that the joint application of these techniques successfully compensates for amplifier nonlinearity, corrects transmission errors even in severely noisy environments (achieving near-perfect image reconstruction at SNR > 10 dB over Rayleigh fading channels), and significantly reduces the data volume without compromising throughput. Furthermore, the rapid convergence of the ALISTA algorithm offsets the additional LDPC decoding complexity, validating the real-time feasibility of the proposed approach. The proposed framework thus enables OTFS systems to simultaneously achieve high data rates, low error rates, and energy efficiency, making it a strong candidate for future 6G communication systems.

Keywords

HPA, OTFS, PAPR, Predistortion, Compressive Sensing, ANN, LDPC

*Correspondence: Hariniony Bienvenu Rakotonirina (dao.rakotonirina@gmail.com)

Received: 19 October 2026; **Accepted:** 28 October 2026; **Published:** 11 November 2026

Copyright: © The Author(s), 2026. Published by Science Publishing Group. This is an **Open Access** article, distributed under the terms of the Creative Commons Attribution 4.0 License (http://creativecommons.org/licenses/by/4.0/), which permits unrestricted use, distribution and reproduction in any medium, provided the original work is properly cited.

1. Introduction

The exponential growth of wireless communication applications, such as the Internet of Things (IoT), autonomous vehicles, and high-speed railway systems, imposes increasingly stringent requirements on modern telecommunication networks, which must operate reliably in highly dynamic environments characterized by significant Doppler shifts and multipath propagation, commonly referred to as doubly selective channels. In such scenarios, OFDM (Orthogonal Frequency Division Multiplexing) modulation, widely adopted in 4G and 5G networks, exhibits severe performance degradation due to inter-carrier interference (ICI) caused by time-varying channel conditions. To address these limitations, OTFS (Orthogonal Time Frequency Space) modulation has recently emerged as a promising waveform for next-generation wireless communications, particularly for 6G networks, by mapping information symbols in the delay-Doppler domain, where the channel representation is typically sparse and quasi-static, thereby enabling full exploitation of channel diversity. However, the practical deployment of OTFS systems faces several critical challenges: on the one hand, as a multi-carrier modulation scheme, OTFS signals exhibit a high Peak-to-Average Power Ratio (PAPR), making them particularly sensitive to the nonlinear distortions introduced by the High-Power Amplifier (HPA) at the transmitter, which causes spectral regrowth, adjacent channel interference, and an increased Bit Error Rate (BER) at the receiver; on the other hand, the growing demand for high-data-rate services necessitates efficient compression techniques to reduce the volume of transmitted information without compromising reconstruction quality, while the inherently noisy transmission channel requires robust error correction mechanisms to ensure reliable data recovery. Although various techniques have been individually proposed in the literature—Digital Predistortion (DPD) to compensate for HPA nonlinearities, Compressive Sensing (CS) to reduce the sampling rate and data volume, and Low-Density Parity-Check (LDPC) codes for their excellent error correction capabilities approaching the Shannon limit—the joint optimization of these techniques within an OTFS framework remains largely unexplored, representing a significant research gap. In this context, this paper proposes a comprehensive optimization of the OTFS transmission system by synergistically combining three complementary techniques: neural network-based predistortion to linearize the HPA and improve power efficiency, Compressive Sensing based on the Lifting Wavelet Transform (LWT) and the ALISTA algorithm to drastically reduce the data volume (down to 10%-30% of the original signal), and LDPC coding to ensure robust transmission even in severely noisy environments, building upon our previous work that has separately demonstrated the effectiveness of each of these approaches.

2. OTFS Modulation

OTFS is an advanced modulation technique particularly well-suited for highly time- and frequency-selective channels, especially in high-mobility environments. Unlike conventional modulation schemes such as OFDM, which map symbols to the time-frequency domain, OTFS maps symbols to the delay-Doppler domain.

2.1. Fundamentals of OTFS Modulation

Figure 1 illustrates the principle of OTFS modulation.

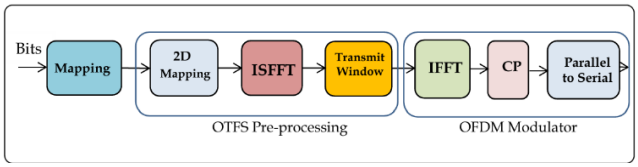


Figure 1. *OTFS modulation.*

Step 1: Mapping

Conversion of bits into complex symbols using single-carrier modulation QPSK, 16-QAM,...

Step 2: 2D Mapping in the Delay–Doppler Domain

The complex symbols are placed on a 2D grid:

1) Horizontal axis: delay index l (temporal delay)

2) Vertical axis: Doppler index k (frequency shift)

Data is organized in the delay–Doppler domain, not in the time or frequency domain.

Step 3: ISFFT (Inverse Symplectic Finite Fourier Transform)

This transformation converts the symbols $x\ [k,l]$ from the delay–Doppler domain into the time–frequency domain $X\ [n,m]$. [1-5, 16].

$$X\ [n,m] = \frac{1}{\sqrt{MN}} \sum_{l=0}^{M-1} \sum_{k=0}^{N-1} x\ [k,l] e^{j2\pi(\frac{nk}{N} - \frac{ml}{M})} \quad (1)$$

l: Delay index

k: Doppler index

n: Time index

m: Frequency index

Step 4: Transmit Window

Filter the signal to reduce sidelobes and inter-symbol interference (ISI).

Step 5: IFFT (Inverse Fast Fourier Transform)

OFDM modulation

Step 6: CP (Cyclic Prefix)

Append a copy of the beginning of the symbol to its end. This is a standard technique in an OFDM system, which prevents inter-symbol interference.

Step 7: Parallel to Serial

The time-domain samples are serialized to form a continuous time signal.

Figure 2 illustrates the principle of OTFS demodulation.

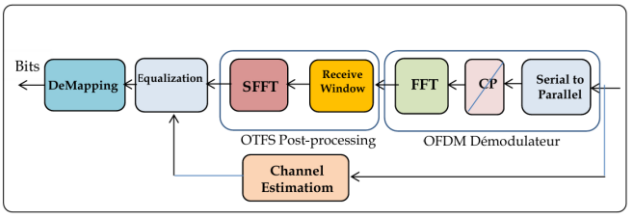


Figure 2. *OTFS demodulation.*

Step 1: Serial to Parallel

Conversion of the serial stream into parallel.

Step 2: Removal of the Cyclic Prefix

The cyclic prefix, which was added at transmission to avoid inter-symbol interference, is removed here.

Step 3: FFT (Fast Fourier Transform)

Converts the time-domain signal into the frequency domain.

Step 4: Receive Window

Filtering to reduce spectral leakage and smooth transitions between symbols.

Step 5: SFFT (Symplectic Finite Fourier Transform)

Converts the data from the time–frequency domain $Y[n,m]$ into the delay–Doppler domain $y[k,l]$.

Step 6: Channel Estimation

Channel estimation is performed using pilot symbols inserted at transmitter. A pilot symbol is a symbol known in advance by both the transmitter and the receiver. By comparing the transmitted and received symbols, the channel state can be estimated.

Step 7: Equalization

Using the channel estimate obtained in the previous step, the effects of the channel on the received symbols can be compensated.

Step 8: DeMapping

Conversion of the estimated complex symbols into binary bits using QPSK, QAM,... demodulation.

2.2. PAPR Modeling of OTFS Signal

Multi-carrier signals, such as OTFS signals, are characterized by high amplitude variations. To measure the amplitude variation of the signal, the PAPR (Peak to Average Power Ratio) is used. Indeed, when the PAPR is high, the signal exhibits large amplitude variations. Equation (2) provides the general expression for the PAPR. This parameter is defined as the ratio between the peak power (P_{max}) and the average power (P_{moy}) of the signal $S(t)$ over a time interval T:

$$PAPR = \frac{P_{max}}{P_{moy}} = \frac{\max_{t\in[0,T]} |S(t)|^2}{\frac{1}{T}\int_0^T |S(t)|^2 dt} \quad (2)$$

To evaluate the PAPR, the CCDF is used. This function gives the probability that the PAPR exceeds a threshold value ψ, and is expressed by Equation 3.

$$CCDF(\psi) = \Pr[PAPR \geq \psi] \quad (3)$$

For OTFS signal, the CCDF is given by Equation (4):

$$CCDF(\psi) = 1 - \left(1 - e^{-\psi}\right)^{NM} \quad (4)$$

where:

M: number of points along the Doppler axis

N: number of points along the delay axis

From Figure 3, we deduce that the OTFS signal (multi-carrier) has a higher probability of exhibiting a high PAPR than the 16-QAM signal (single-carrier).

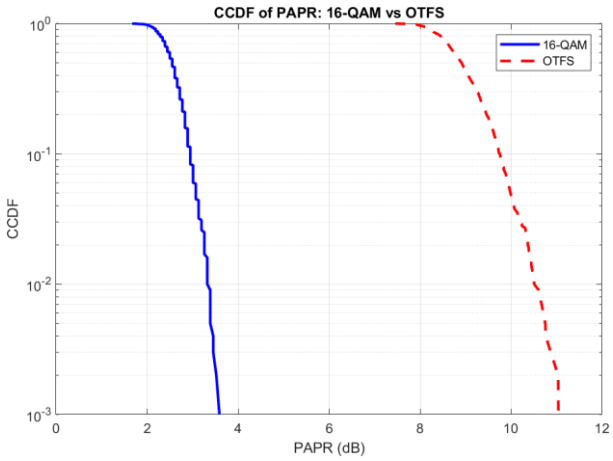


Figure 3. *CCDF of PAPR: 16-QAM vs OTFS.*

2.3. Amplification of OTFS Signal

The curve showing the variation of output power as a function of input power of a power amplifier is also referred to as the AM/AM characteristic. It exhibits a typical shape for all amplifiers (see Figure 4).

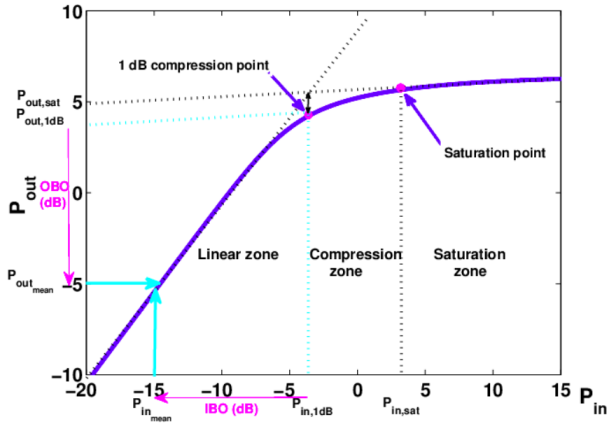


Figure 4. *AM/AM characteristics.*

The AM/AM characteristic of a power amplifier is divided into three regions [6-16]:

1) *Linear zone:* In this region, the amplifier exhibits linear behavior. The output power is proportional to the input power, with the proportionality factor known as the amplifier gain. Input power levels are low. In this region, distortions caused by nonlinearity are nonexistent. When operating with sufficient back-off to avoid distortions, the amplifier functions within this linear region.
2) *Compression zone:* In this region, output power is no longer proportional to input power. The curve begins to bend, marking the onset of nonlinear behavior. Signal distortions appear and become increasingly significant as input power rises. The amplifier gain decreases for high input power levels, which is why this region is referred to as the gain compression region. The 1-dB gain compression point lies within this region; it is defined as the point where the difference between the actual gain curve and the ideal linear gain equals 1 dB. This point is a key characteristic of the power amplifier.
3) *Saturation zone:* In this region, the output power remains nearly constant regardless of further increases in input power. This constant output power level is referred to as the saturation power, which is another fundamental characteristic of the power amplifier.

The curve showing phase shift as a function of input amplitude is called the AM/PM transfer characteristic. It has no standard shape; it varies depending on the amplifier's design technique and operating conditions.

In short, amplification is a nonlinear operation characterized by amplitude compression (AM/AM) and phase shift at the output (AM/PM).

The nonlinearity of a power amplifier causes distortion of the amplified signal, especially when the signal exhibits large amplitude variations. Indeed, these distortions result in transmission errors (Figures 5-6) and spectral regrowth, which can cause interference (Figure 7).

channel

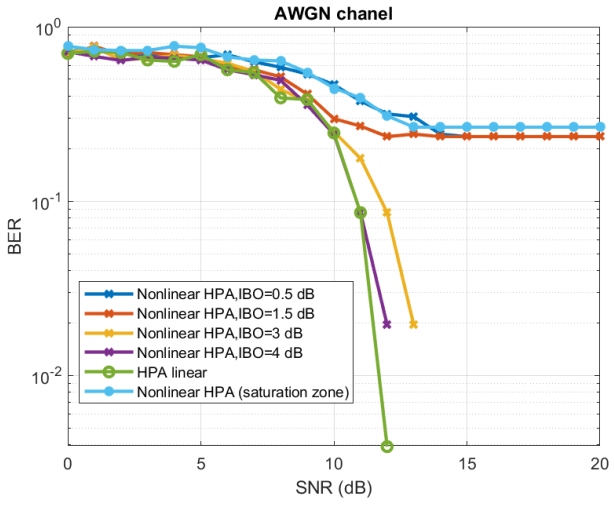


Figure 5. *BER over AWGN Channel.*

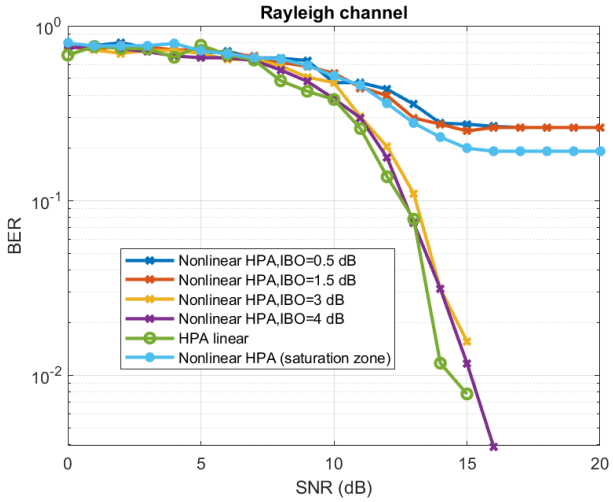


Figure 6. *BER over Rayleigh Channel.*

All curves exhibit a high BER at low SNR, followed by a rapid decrease as the SNR increases.

The BER after linear amplification (green curve) is the lowest, as it represents an ideal amplifier without nonlinear distortion.

The BER after nonlinear amplification (light blue curve) remains very high even at high SNR. Nonlinear amplification thus saturates the signal and causes significant information loss.

We also observe that a higher IBO (Input Back Off) significantly improves the BER: the higher the IBO, the closer the amplifier operates to its linear region. To avoid or at least mitigate the detrimental effects caused by amplifier nonlinearity, the amplifier is often oversized i.e., operated with a certain amount of back-off to ensure operation within or near the linear region. This back-off is typically referenced either to the 1-dB compression point or to the saturation power level. Input Back-Off (IBO), typically expressed in dB, is the ratio between the input-referred saturation power $P_{in,sat}$ and the actual input signal power P_{in}, or alternatively, the ratio between the input power at the 1-dB compression point $P_{in,1dB}$ and the actual input signal power P_{in}.

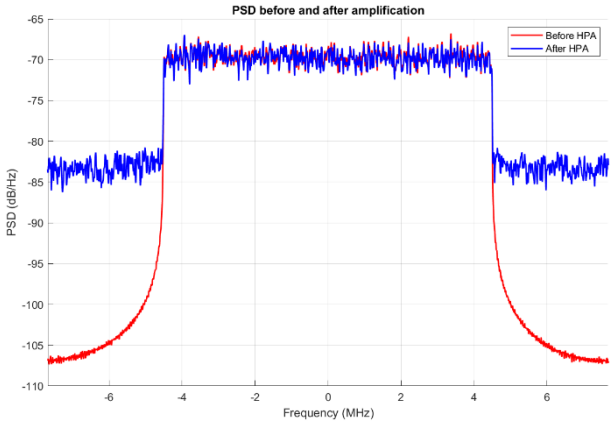


Figure 7. *PSD before and after amplification.*

Table 1. ACRP before and after amplification.

ACPR before HPA	ACPR after HPA
-37 dB	-15 dB

From these results, we deduce that the signal spectrum before amplification is well confined within the useful bandwidth (approximately ±4 MHz). The side lobes decay rapidly. Indeed, the ACPR before amplification is -37 dB. We conclude that, prior to amplification, the signal spectrum is very clean, with minimal interference in adjacent channels.

After amplification, a significant increase in spectral noise is observed in the adjacent bands. Moreover, the shape of the spectrum within the main band is slightly distorted. The ACPR after amplification is -15 dB, meaning that the power in the adjacent channel has increased by 22 dB hence, the risk of interference with neighboring channels increases significantly.

3. Optimizing the Performance of OTFS Communication Systems

The primary objectives of modern telecommunications are:

1) Ensuring reliable data transmission, even in noisy environments.
2) Achieving high-data-rate transmission.
3) Promoting green communication, characterized by low system energy consumption.

To meet these objectives, we propose the following enhancements for the OTFS transmission system. Figure 8 presents the proposed enhancements to the OTFS transmission system:

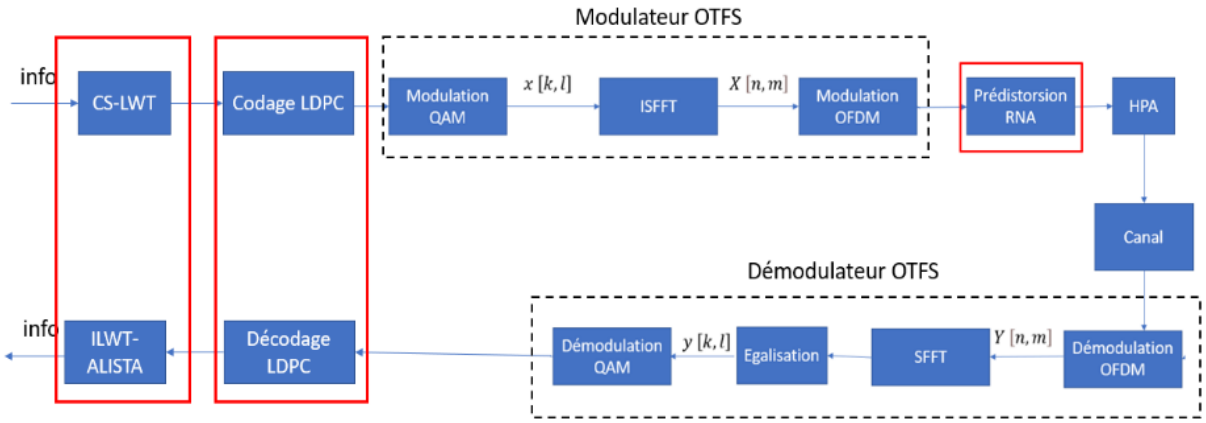


Figure 8. Optimized OTFS Transmission System.

The High-Power Amplifier (HPA) is a crucial component in the transmission system, as it amplifies the signal power prior to transmission. As a multicarrier signal, OTFS exhibits significant amplitude variations. Amplifying such a signal introduces nonlinear distortions, which manifest as an increased Bit Error Rate (BER), adjacent channel interference, and higher power consumption of the amplifier. To address these issues, we have previously demonstrated the effectiveness of a neural network-based predistortion technique in a prior study [16]. This technique enables the amplifier to operate with high efficiency (i.e., low power consumption) without introducing distortions to the amplified signal.

One of the primary objectives of modern telecommunications is achieving high-data-rate transmission. Consequently, we sought a method to reduce the volume of transmitted data while guaranteeing its accurate reconstruction at the receiver. To this end, we decided to integrate Compressive Sensing (CS) into the OTFS transmission system. We have demonstrated in several studies [17-20] that CS based on the Lifting Wavelet Transform (LWT) and the ALISTA algorithm enables accurate signal reconstruction even from a highly reduced number of samples (e.g., 10% or 20% of the original signal). Furthermore, the reconstruction time is remarkably fast. The utilization of the CS-LWT-ALISTA technique successfully fulfills our high-throughput objectives.

After amplification, the signal propagates through the transmission channel, which is subject to noise. This noise introduces signal distortions and increases the BER at the receiver. To mitigate this issue, we have incorporated Low-Density Parity-Check (LDPC) coding into the OTFS system. Specifically, the signal samples obtained after compressive sensing are processed by an LDPC encoder to enhance their robustness against channel noise [21, 22].

3.1. Simulation Parameters

Table 2. Summarizes the simulation parameters.

Mapping	4 QAM
Sampling rates M (compressive sensing)	10% to 60%
Amplifier model	Rapp
Reconstruction algorithm	ALISTA
LDPC code rate	1/2, 1/3, 1/4
Measurement matrix ϕ	Gaussian measurement matrix $M \times 40000$
Data	Image (Lena excerpted from the original publication: A. K. Jain, Fundamentals of Digital Image Pro-cessing, Prentice-Hall, 1989, p. 400. Original source: photograph from Play-boy magazine, No-vember 1972. Used here for non-commercial ed-ucational and re-search purposes)
Sparse representation	LWT
Wavelet	Db7
Transmission channel	AWGN, Rayleigh
SNR	-20dB à20dB
Hardware specifications	CPU: Intel (R) Core i7-9750H, GPU: NVIDIA GetForce RTX 2060, RAM: 16Go
Programming environment	MATLAB 2023

Architecture of the neural network used:

An input layer comprising a single neuron. Indeed, since the neural network has only one input, a single neuron in the input layer is appropriate. A hidden layer with ten neurons using the hyperbolic tangent activation function. This activation function allows us to randomly initialize the synaptic weights during training, thereby accelerating the convergence of the learning algorithm. An output layer consisting of a single neuron with a linear activation function. In this study, we employed Levenberg-Marquardt learning algorithms.

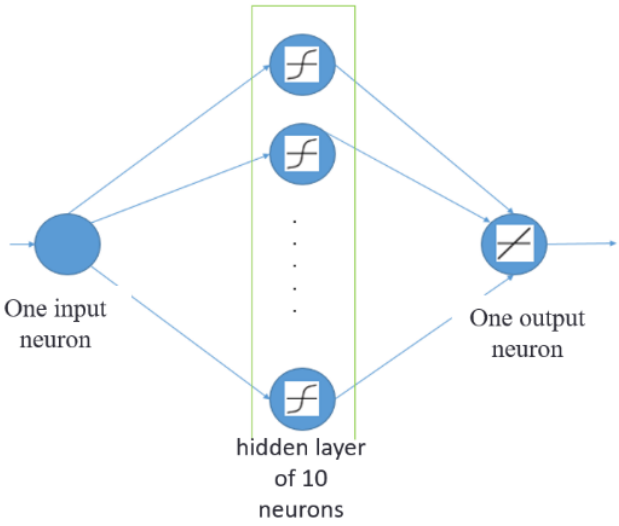


Figure 9. Architecture of the neural network used.

3.2. Results

The SSIM and the image reconstruction time were adopted as performance criteria.

3.2.1. SSIM vs. SNR

The SSIM and the image reconstruction time were adopted as performance criteria.

Figures 10 and 11 show the SSIM versus SNR for a 30% sampling rate, i.e., only 30% of the data is transmitted.

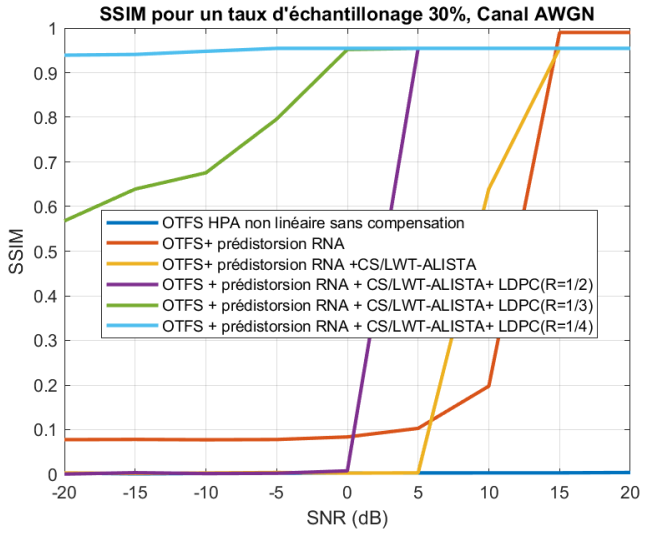


Figure 10. *SSIM vs. SNR AWGN channel.*

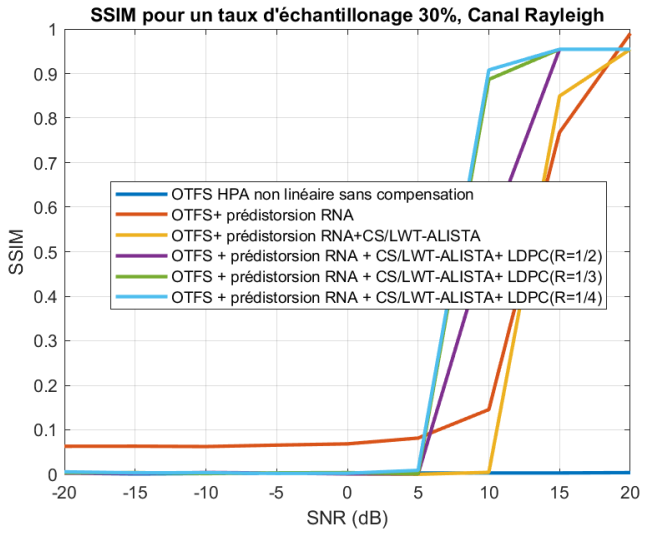


Figure 11. *SSIM vs. SNR Rayleigh channel.*

Without HPA nonlinearity compensation, the SSIM remains virtually zero regardless of the SNR value, demonstrating that nonlinear distortions alone destroy all useful information. Neural network-based predistortion effectively compensates for the amplifier's nonlinearity but does not eliminate the noise and interference introduced by the channel. Consequently, this technique yields an SSIM close to 1 only at high SNR levels (SNR > 15 dB).

Combining Compressive Sensing (CS/LWT-ALISTA) with neural network-based predistortion improves the quality of the received image even at moderate noise levels (SNR between 5 dB and 12 dB). However, the performance of this combined approach degrades in highly noisy channels. Integrating LDPC coding into this framework further enhances image reconstruction, even in noisy environments.

For the AWGN channel, a code with a rate of R=1/4 enables successful image reconstruction even at an SNR of -20 dB. A code rate of 1/3 achieves optimal performance at an SNR of 0 dB, while an SNR of 5 dB is required for a code rate of 1/2 to accurately reconstruct the image.

In a Rayleigh fading channel, LDPC coding effectively corrects transmission errors as soon as the SNR exceeds 5 dB. Furthermore, code rates of 1/3 and 1/4 achieve near-perfect image reconstruction when the SNR is greater than 10 dB.

In summary, the joint application of neural network-based predistortion, CS (LWT-ALISTA), and LDPC coding successfully compensates for amplifier nonlinearity, corrects transmission errors even in noisy environments, and significantly reduces the volume of data to be transmitted (in this case, transmitting only 30% of the original data).

3.2.2. SSIM vs. Sampling Rates *M*

Figures 12 to 15 illustrate the SSIM versus the sampling rate.

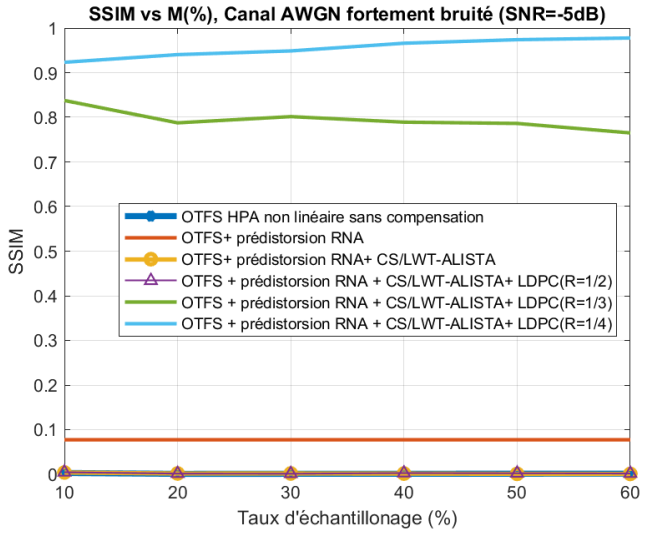


Figure 12. *SSIM vs Sampling rates M AWGN channel (SNR=-5dB).*

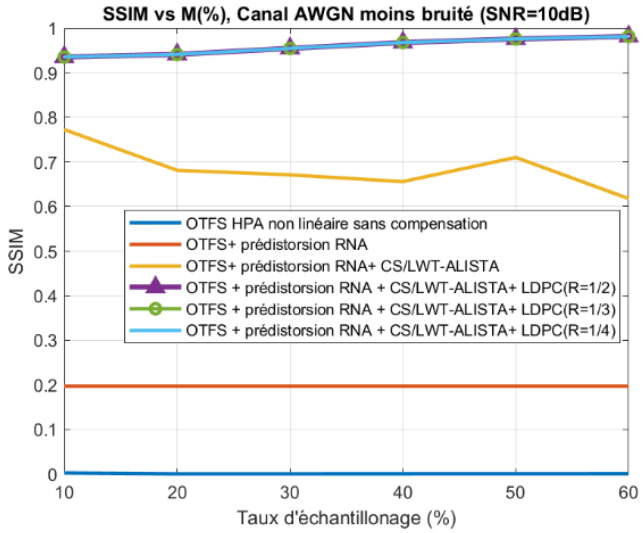


Figure 13. *SSIM vs Sampling rates M AWGN channel (SNR=10dB).*

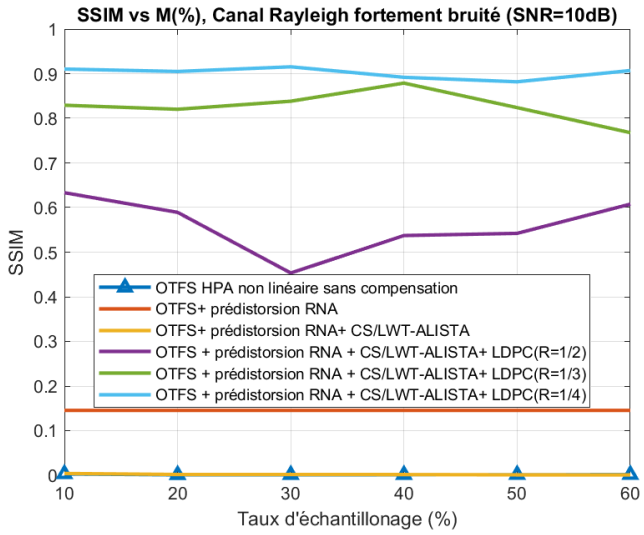


Figure 14. *SSIM vs Sampling rates M Rayleigh channel (SNR=10dB).*

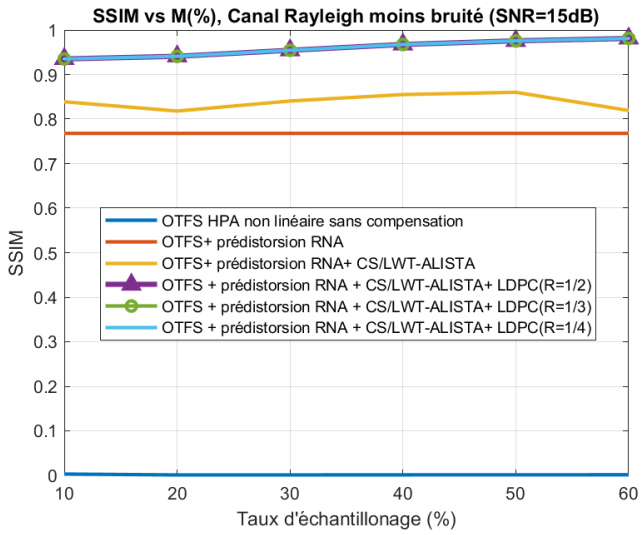


Figure 15. *SSIM vs Sampling rates M Rayleigh channel (SNR=15dB).*

It can be concluded that employing a code rate of 1/4 guarantees reliable image reconstruction, even in a highly noisy environment. However, using such a code reduces the transmission throughput, as it introduces significant redundancy into the data. Conversely, a code rate of 1/2 doubles the data rate provided by a 1/4 code rate. Nevertheless, this higher-rate code is insufficient to protect the data in a severely noisy channel.

This is precisely where the integration of CS (LWT-ALISTA) becomes essential. Compressive Sensing reduces the volume of data to be transmitted (e.g., M=10%, 20% or 30%). Consequently, the bandwidth saved by CS is reallocated to the redundancy bits introduced by the LDPC coding. Therefore, in a moderately noisy environment, a code rate of 1/2 is sufficient to correct transmission errors. Conversely, in a severely noisy environment, a code rate of 1/4 is required, and CS offsets the redundancy introduced by the LDPC code, thereby preventing any degradation in the overall data rate.

In summary, through the joint application of neural network-based predistortion, CS (LWT-ALISTA), and LDPC coding, the OTFS system can simultaneously achieve a high data rate and a low error rate, even in severely noisy environments.

3.2.3. Image Reconstruction Time vs. Sampling Rates *M*

Figure 16 illustrates the data reconstruction time versus the sampling rate.

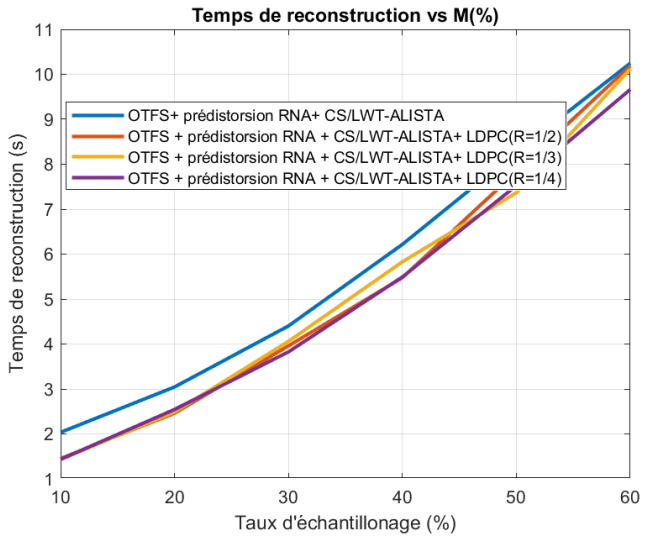


Figure 16. *Reconstruction time vs. Sampling rates M.*

It can be deduced that as the sampling rate increases, the volume of data to be processed grows proportionally. This results in an increase in computational complexity, which justifies the advantage of employing a low sampling rate (e.g., 10%, 20%, or 30%). The system without LDPC exhibits a longer reconstruction time. Although LDPC coding

adds a layer of complexity to the OTFS system (incorporating neural network-based predistortion and CS/LWT-ALISTA), it enables the correction of transmission errors prior to image reconstruction. Consequently, the ALISTA algorithm converges more rapidly. This rapid convergence of the ALISTA algorithm significantly offsets the LDPC decoding time.

4. Originality and Our Contribution to the Research

The main contributions of this work are summarized as follows:

1) Proposing a neural network model to linearize the power amplifier in an OTFS transmission system.
2) Optimizing the performance of an OTFS transmission system through the joint integration of three techniques: neural network-based predistortion, LWT/ALISTA-based compressive sensing, and LDPC coding.

5. Conclusions

This paper has presented a comprehensive optimization of the OTFS transmission system by synergistically combining three complementary techniques: neural network-based predistortion, Compressive Sensing based on the Lifting Wavelet Transform (LWT) and the ALISTA algorithm, and LDPC coding. This joint approach simultaneously addresses the three primary objectives of modern telecommunications: transmission reliability, high data rate, and energy efficiency. Simulation results have demonstrated that neural network-based predistortion effectively compensates for the nonlinearities of the High-Power Amplifier (HPA), enabling it to operate with high efficiency while preserving signal quality. The integration of Compressive Sensing significantly reduces the volume of data to be transmitted (down to 10%-30% of the original signal), thereby freeing up bandwidth that can be reallocated to the redundancy bits of LDPC coding. The latter ensures robust correction of transmission errors, even in severely noisy environments, achieving near-perfect image reconstruction for signal-to-noise ratios above 10 dB in a Rayleigh fading channel. The analysis of reconstruction time has revealed that the rapid convergence of the ALISTA algorithm significantly offsets the LDPC decoding time, thus validating the real-time feasibility of the proposed approach. Furthermore, the use of low sampling rates (10%, 20%, or 30%) significantly reduces the computational complexity of the system. In summary, the combination of these three techniques enables the OTFS system to simultaneously achieve a high data rate, a low error rate, and reduced energy consumption, even under severe channel conditions. These results open promising prospects for the deployment of 6G communication systems tailored for high-mobility environments. Future work may explore the extension of this approach to other waveforms and the joint optimization of the three techniques' parameters for even more complex channel scenarios.

Abbreviations

6G	Sixth Generation of Mobile Communications
ACPR	Adjacent Channel Power Ratio
AM	Amplitude
ANN	Artificial Neural Network
AWGN	Additive White Gaussian Noise
BER	Bit Error Rate
CCDF	Complementary Cumulative Distribution Function
CP	Cyclic Prefix
FFT	Fast Fourier Transform
HPA	High Power Amplifier
IBO	Input Back-Off
IFFT	Inverse Fast Fourier Transform
ISFFT	Inverse Symplectic Finite Fourier Transform
LSTM	Long Short-Term Memory
OBO	Output Back-Off
OFDM	Orthogonal Frequency Division Multiplexing
OTFS	Orthogonal Time Frequency Space
PAPR	Peak-to-Average Power Ratio
PM	Phase
QAM	Quadrature Amplitude Modulation
SFFT	Symplectic Finite Fourier Transform
SSIM	Structural Similarity Index Measure
SNR	Signal-to-Noise Ratio

Author Contributions

Hariniony Bienvenu Rakotonirina: Conceptualization, Formal Analysis, Investigation, Methodology, Project administration, Resources

Randriana Heritiana Nambinina Erica: Conceptualization, Formal Analysis, Investigation, Methodology, Project administration, Resources

Marie Emile Randrianandrasana: Supervision, Validation

Ando Nirina Andriamanalina: Supervision, Validation

Data Availability Statement

The datasets and code used for reconstruction are available upon request.

Conflicts of Interest

The authors declare no conflicts of interest.

References

[1] Elakkiyachelvan, E., Kavitha, R., J., (2022). Space-Time Coding and LMMSE Receiver in OTFS Modulation. Proc. ITSPWC 2022. https://doi.org/10.4108/eai.14-5-2022.2318877

[2] Sura H., Thamer M., Hassan F., (2025). A Performance and Evaluation of OTFS Modulation Systems Using Different High Mobility Channels. Int. J. Electronics & Telecommunication, 71(2), pp. 505-512. https://doi.org/10.24425-ijet.2025.153598

[3] Obinna, O., Xutao, D., Agbotiname, L., Olamilekan, S., (2025). OTFS: A Potential Waveform for Space-Air-Ground Integrated Networks in 6G and Beyond. Telecom, 6(1), 19. https://doi.org/10.3390/telecom6010019

[4] Franz, L., Hamdi, J., Alex, A., Frans, M. J., (2022). Orthogonal Time-Frequency Space Modulation Based on the Discrete Zak Transform. Entropy, 24(12), 1704. https://doi.org/10.3390/e24121704

[5] Wei, L., Xuan, L., Jia, S., Lixin, L., Junfan, H., (2022). Underlying Security Transmission Design for OTFS Modulation. Sensors, 22(20), 7919. https://doi.org/10.3390/s22207919

[6] Li, W., Montoro, G., & Gilabert, P. L. (2025). Adaptive Digital Predistortion for User Equipment Power Amplifiers Under Dynamic Frequency, Bandwidth, and VSWR Variations. IEEE Transactions on Microwave Theory and Techniques, PP (99): 1-13. https://doi.org/10.1109/TMTT.2025.3563159

[7] Wu, Y., Li, A., Beikmirza, M., Singh, G. D., Chen, Q., de Vreede, L. C. N., Alavi, M., & Gao, C. (2024). MP-DPD: Low-Complexity Mixed-Precision Neural Networks for En-ergy-Efficient Digital Predistortion of Wideband Power Amplifiers, IEEE Microwave and Wireless Technology Letters, https://doi.org/10.1109/LMWT.2024.3386330

[8] Spano, C., Badini, D., Cazzella, L., & Matteucci, M. (2025). Local and Remote Digital Pre-Distortion for 5G Power Amplifiers with Safe Deep Reinforcement Learning. *Sensors*, 25(19), 6102. https://doi.org/10.3390/s25196102

[9] Thys, C., Martinez Alonso, R., Lhomel, A., Fellmann, M., Deltimple, N., Rivet, F., & Pollin, S. (2024). Walsh-domain Neural Network for Power Amplifier Behavioral Modelling and Digital Predistortion. IEEE International Symposium on Circuits and Systems (ISCAS), https://doi.org/10.1109/ISCAS58744.2024.10557970

[10] Kostrzewska, K., & Kryszkiewicz, P. (2024). Power Amplifier Modeling Framework for Front-End-Aware Next-Generation Wireless Networks. Electronics, Mdpi. https://doi.org/10.3390/electronics13091643

[11] Galaviz-Aguilar, J. A., Vargas-Rosales, C., Cárdenas-Valdez, J. R., Aguila-Torres, D. S., Flores-Hernández, L. (2022). A Comparison of Surrogate Behavioral Models for Power Amplifier Linearization under High Sparse Data. *Sensors*, 22(19), 7461. https://doi.org/10.3390/s22197461

[12] Kang, M., Lim, S., Park, Y. (2023). Deep Neural Network for the Behavioral Modeling of Memory Effects and Supply Dependency on 10-W Nonlinear Power Amplifiers. Journal of Electromagnetic Engineering and Science, 23(2), 134-138. https://doi.org/10.26866/jees.2023.2.r.152

[13] Ortali, J., Mons, S., Reveyrand, T., Ngoya, E., & Mazière, C. (2025). Behavioral Modeling of RF Power Amplifiers Using a Time-Domain Characterization Approach. International Journal of Microwave and Wireless Technologies, 17(S6), 942-949. https://doi.org/10.1017/S175907872500042X

[14] Tang, X., Wang, Z., Wang, Y. (2024). A Wideband Behavioral Model with Multiple States for RF Power Amplifier Based on Improved Recurrent Neural Network. 2024 2nd International Symposium of Electronics Design Automation (ISEDA), https://doi.org/10.1109/ISEDA62518.2024.10617555

[15] Vimal, V., Thakur, P., Gupta, S., (2025). RF-Power Amplifier Modelling Using Inverse System Identification. Discover Computing, 28, 21. https://doi.org/10.1007/s10791-025-09522-4

[16] Rakotonirina, H. B., Randrianandrasana, M. E. (2025). *Exploitation of Feedforward Neural Networks to Improve HPA Predistortion Performance and Application to OTFS Signals*. Advances in Wireless Communications and Networks, 10(1), 9-27. https://doi.org/10.11648/j.awcn.20251001.12

[17] Luc, S. N. R. F., Randrianandrasana, M. E., Rakotonirina, H. B. (2025). *Image Reconstruction in Compressive Sensing Using Biorthogonal 5.5 (bior5.5) and Lifting Wavelet Transforms with SP, CoSaMP, and ALISTA Algorithms*. Science Journal of Circuits, Systems and Signal Processing, 12(2), 16-29. https://doi.org/10.11648/j.cssp.20251202.11

[18] Luc, S. N. R. F., Randrianandrasana, M. E., Rakotonirina, H. B. (2025). *Image Reconstruction in Compressive Sensing Using Daubechies 7 (db7) and Lifting Wavelet Transforms with SP, CoSaMP, and ALISTA Algorithms.* American Journal of Computer Science and Technology, 8(4), 214-227. https://doi.org/10.11648/j.ajcst.20250804.15

[19] Luc, S. N. R. F., Randrianandrasana, M. E., Rakotonirina, H. B. (2025). *Image Reconstruction in Compressive Sensing Using Reverse Biorthogonal 6.8 (rbio6.8) and Lifting Wavelet Transforms with SP, CoSaMP, and ALISTA Algorithms*. American Journal of Electrical and Computer Engineering, 9(2), 22-35. https://doi.org/10.11648/j.ajece.20250902.12

[20] Luc, S. N. R. F., Randrianandrasana, M. E., Rakotonirina, H. B. (2025). *Image Reconstruction in Compressive Sensing Using Symlet 8 (sym8) and Lifting Wavelet Transforms with SP, CoSaMP, and ALISTA Algorithms*. American Journal of Information Science and Technology, 9(4), 277-290. https://doi.org/10.11648/j.ajist.20250904.12

[21] Moon K., *Error Correction Coding*, 2nd Edition, Wiley, 2020, pp. 637–717.

[22] Sodha J., *Fundamentals of Polar, Ldpc and Turbo Codes: With Matlab and Mathcad Simulations and Desktop Video Lectures*, Springer, 2026, pp. 63–82.

Research Field

Hariniony Bienvenu Rakotonirina: Telecommunication, Signal

processing, Compressive Sensing, Artificial intelligence, High Amplifier Power Nonlinearity

Randriana Heritiana Nambinina Erica: Telecommunication, transmission, optical fiber, optical communication, Signal Processing

Marie Emile Randrianandrasana: Telecommunication, Signal processing, Compressive Sensing, Radar, Electromagnetic wave

Ando Nirina Andriamanalina: Telecommunications, Control Systems, Signal Processing